Nanoscale Horizons

ROYAL SOCIETY OF CHEMISTRY

COMMUNICATION

View Article Online
View Journal | View Issue

Cite this: *Nanoscale Horiz.*, 2021, 6, 348

Received 4th December 2020,
Accepted 22nd February 2021

DOI: 10.1039/d0nh00674b

rsc.li/nanoscale-horizons

Ferroptosis/pyroptosis dual-inductive combinational anti-cancer therapy achieved by transferrin decorated nanoMOF†

Rui Xu, Jie Yang, Yun Qian, Huizi Deng, Zhihua Wang, Siyu Ma, Yawen Wei, Ning Yang and Qi Shen *

Non-apoptotic cell death such as ferroptosis and pyroptosis has shed new light on cancer treatment, whereas combinational therapy using both these mechanisms has not yet been fully explored. Herein, a dual-inductive nano-system to realize ferroptosis/pyroptosis mediated anti-cancer effects is presented. The nanodrug (Tf-LipoMof@PL) is constructed with a piperlongumine (PL) loaded metal–organic framework (MOF) coated with transferrin decorated pH sensitive lipid layer. Intracellular iron was enriched with an iron-containing MOF, whose endocytosis can be further facilitated by transferrin decorated on the lipid layer, which provides a prerequisite for the occurrence of ferroptosis and pyroptosis. Piperlongumine as the ferroptosis inducer can strengthen the ferroptotic cell death, and provide H_2O_2 for the dual induction system to increase ROS generation through Fenton reaction. On the basis of validation of both ferroptosis and pyroptosis, the dual-inductive nanodrug demonstrated ideal anti-cancer effects in the xenograft mice model, which proved that the ferroptosis/pyroptosis dual-inductive nanoplatform could be an effective and promising anticancer modality.

Introduction

Novel cancer therapies continue to be urgently needed due to the problems of existing traditional chemotherapy such as strong side effects and drug resistance.[1–3] Because most chemotherapies induce programmed death of cells through apoptosis,[4] there have been researches on novel cancer therapies to induce cell death other than apoptosis, for example, through multi-functional modality which has become a promising method for novel cancer treatments.[5] In recent years, multiple cell death forms have been discovered and characterized with their corresponding molecular mechanisms which act as stimuli for ferroptosis, pyroptosis, paraptosis, necroptosis and so on, providing new choices for cancer treatment research.[6] Ferroptosis is a unique form of cell death characterized by iron-dependent lipid peroxidation leading to cell membrane injury, which was first found by Dixon *et al.*,[7] and pyroptosis is mediated by caspase-induced gasdermin (GSDM) cleavage with GSDM pore formation followed by cell swelling and bursting.[8,9] Both of these two cell death forms were found to be able to be induced by increased intracellular iron and ROS.[7,10,11] Thus, iron manipulation and ROS elevation may serve as the common stimulus for both ferroptosis and pyroptosis. Although there have already been studies on the application of ferroptosis[12] and pyroptosis[13,14] in anti-cancer therapies, the combination of the both cell death forms has not yet been found in any anticancer modality, and this research may shed new light on novel anti-tumor treatments.

To build up an effective ferroptosis/pyroptosis mediating system, the key point lies in how to increase intracellular iron level and boost iron-related cell death inducing pathways effectively. To tackle these problems, a highly efficient iron donor is required. An iron containing nano metal–organic framework (MOF) is an ideal iron donor and drug delivery system because of its high amount of irons and porous structure.[15] Transferrin is an iron-transport glycoprotein that integrates iron into cells *via* transferrin-receptor (TfR) mediated endocytosis.[16] The combination of an iron-containing MOF and transferrin may lead to enhanced iron endocytosis. Moreover, the upregulated TfR expression on the surface of various tumor cells provides not only natural advantages for more efficient transferrin-mediated iron endocytosis, but also targets for therapeutic drug delivery.[17,18] Thus, the additional transferrin can simultaneously help to capture more Fe^{3+} in the tumor cells and accelerate the TfR mediated endocytosis circulating procedure. In addition, the increased intracellular iron can lead to lethal ROS generation through the Fenton reaction which has been reported to have strong relationships with cancer development.[11,19] Therefore, simultaneously increasing

School of Pharmacy, Shanghai Jiao Tong University, 800 Dongchuan Road, Shanghai 200240, China. E-mail: qshen@sjtu.edu.cn; Fax: +86-21-34204049; Tel: +86-21-34204049

† Electronic supplementary information (ESI) available. See DOI: 10.1039/d0nh00674b

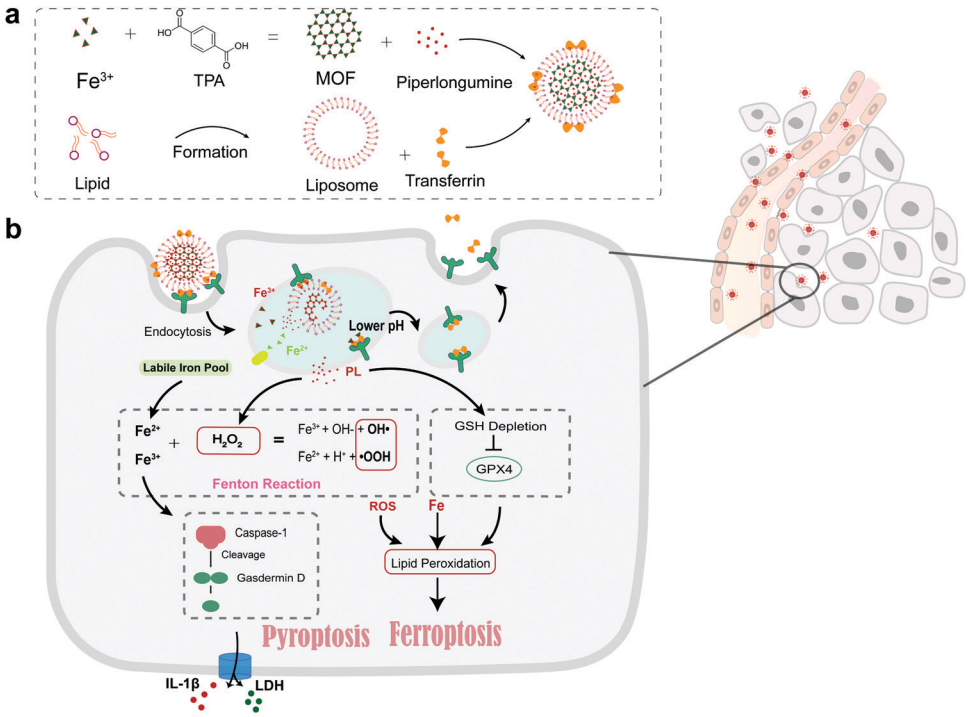

Scheme 1 (a) Formation of the Tf-LipoMof@PL nanoparticles. (b) The illustration of the mechanism of the nanoparticles.

all the reactants of Fenton reaction (iron and H_2O_2) can enhance lethal ROS production, thus subsequently facilitating both pyroptosis and ferroptosis.

Thus, a highly efficient ferroptosis/pyroptosis dual-inductive nano delivery system Tf-LipoMof@PL, in which piperlongumine (PL, an effective ferroptosis inducer) was loaded in iron-containing MOFs coated with a DOPE pH sensitive lipid layer with transferrin decoration was created, which is shown in Scheme 1a. As Scheme 1b suggests, intracellular iron can be modulated by iron-containing MOFs and transferrin, and H_2O_2 can be provided by PL, whose combination can trigger Fenton reaction leading to increased intracellular ROS. Both effects can evoke ferroptosis and pyroptosis. Meanwhile, the GSH decreasing ability of PL can further induce ferroptosis.[20] Hence, the aim of this work was to simultaneously induce ferroptosis and pyroptosis by modulating intracellular iron and ROS by Tf-LipoMof@PL nanocarriers.

Results and discussion

Characterization of the nanoparticles

To build the designed nano-system, the nanosized MOF was synthesized as reported previously.[21] To enhance cellular uptake, prevent early drug leakage and realize pH responsive drug release in response to a low pH at the tumor site, the nanoMOF was coated with a DOPE-pH sensitive lipid layer. Coating was performed by incubating the MOF with DOPE liposomes (v/v = 1 : 1). Transferrin was embedded on the lipid layer by mixing fresh transferrin with liposomes. The resulting hydrodynamic radius of Tf-LipoMof@PL measured by DLS was 185 ± 5.7 nm, whereas that of the Mof@PL was about 172 ± 6.2 nm (Fig. 1a). The surface charge of the nanoparticles changed from +45 ± 2.8 mV to −10.2 ± 0.6 mV because of the coated lipid layer (Fig. 1b). Images of the transmission electron microscopy (TEM) of MOF and Tf-LipoMof nanoparticles were displayed in Fig. 1c, and these showed that the lipid layer was about 10 nm which was in agreement with the radius difference of Tf-LipoMof@PL and Mof@PL found in DLS results. Successful coating was confirmed by the results of a fluorescence release experiment (Fig. S1, ESI†). An isotherm of unfunctionalized nanoMof and LipoMof was shown in Fig. S2 (ESI†). The decrease in surface area for LipoMof confirmed that the successful lipid-coating was due to the pore blocking ability of the lipid, which can prevent early drug leakage. X-ray powder diffraction (XRD) patterns of uncoated Mofs and decorated NanoMofs were presented in Fig. S3 (ESI†). Fourier-transform infrared (FTIR) spectroscopy images also showed no obvious differences between the groups (Fig. 1d). The same diffraction pattern of transferrin and lipid layer decorated Mof suggested that the Mof structures were stable during the lipid coating procedure. By comparing the TEM results (Fig. S4, ESI†), the nanoparticles were clearly ruptured at pH 5.5 after 30 min whereas stayed intact at pH 7.4, suggesting the establishment of the pH sensitive response system. The embedding efficiency of transferrin was 73.6 ± 3.48% confirmed by BCA analysis. The encapsulation efficiency of PL was 78.7 ± 2.98% and the loading efficiency was 12.3 ± 4.33%. The amount of Fe was 6.8 ± 0.07 mM in 1 mg of lyophilized LipoMof measured by an intracellular iron colorimetric assay kit. Release behaviors of PL in PBS of pH 7.4 or sodium citrate buffer of pH 5.5 to simulate the pH in physiological blood and the acidic environment of

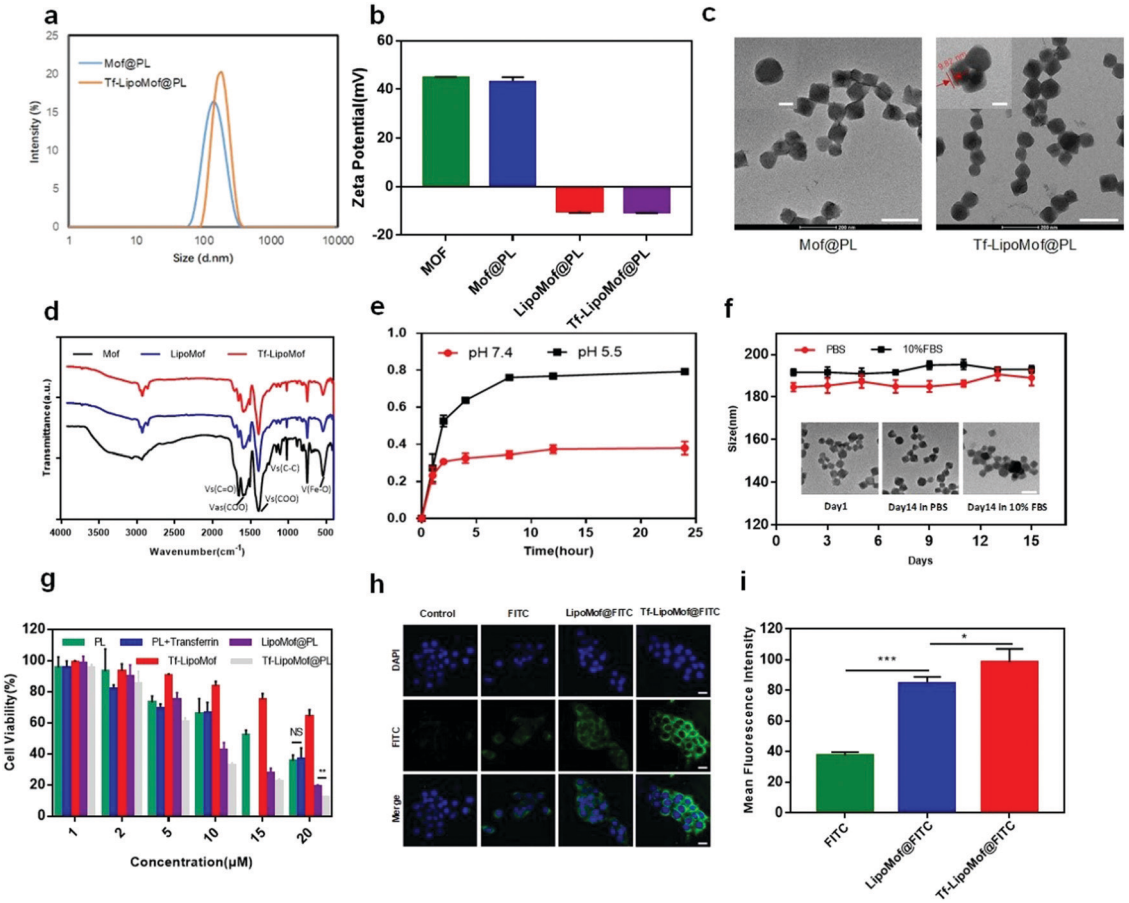

Fig. 1 (a) Hydrodynamic size of Mof@PL and Tf-LipoMof@PL. (b) Zeta potential of Mof@PL and Tf-LipoMof@PL (bar = 200 nm). (c) The TEM images of Mof@PL and Tf-LipoMof@PL. (d) The FTIR spectroscopy spectra of Mof, LipoMof and Tf-LipoMof. (e) Piperlongumine release profile (n = 3). (f) Size and morphology stability of nanoparticles. (g) Cytotoxicity of different formulations at various piperlongumine concentrations (1, 2, 5, 10, 15, 20 μM) in 4T1 cells. (h and i) LSCM images and semi-quantification for cellular uptake of the nanoparticles.

tumor site, respectively, were assessed. At pH 5.5, there was about 55.6% of total PL released in the first 4 h and 82.5% PL was released after 24 h, whereas only about 32.1% PL was readily released at pH 7.4 (Fig. 1e). The release behavior of the Fe ions was also evaluated in PBS of pH 7.4 and pH 5.5 (Fig. S5, ESI†). In accordance with the PL release behavior, 88.1% of Fe ions were released in pH 5.5 medium in 24 h whereas only 17.6% was released in the pH 7.4 medium. This reinforced the successful establishment of the whole pH-sensitive drug delivery system and limited premature drug release. The stability of the Tf-LipoMof@PL nanoparticles were examined by a long term storage test. The Tf-LipoMof@PL nanoparticles were stored in PBS (pH 7.4) and 10% FBS for 14 days at 4 °C. The DLS diameter and TEM images obtained suggested that the nanoparticles were stable in PBS and 10% FBS (Fig. 1f).

In vitro analysis of nanoMofs

A preliminary examination was made to assess the *in vitro* cytotoxicity of the free drug and drug-loaded nanoparticles on 4T1 cells. After treatment with different formulations with various drug concentration ladders, as Fig. 1g showed, the cell viability of 4T1 cells was diminished in a dose-dependent way. When the drug concentration was increased, Tf-LipoMof@PL showed the strongest cytotoxicity compared with other groups. In addition, free transferrin made no difference to cytotoxicity because the PL + transferrin group presented nearly the same cytotoxicity with free PL, suggesting there were no synergistic effects between free PL and transferrin. There was statistical significance shown between the LipoMof@PL group and the Tf-LipoMof@PL group at 20 μM, suggesting transferrin's contribution to the cytotoxicity of Tf-LipoMof@PL which was produced by the combinational effects of transferrin and Mof@PL. It was presumed that the increase of cytotoxicity produced by transferrin was due to its ability in enhancing endocytosis by targeting the receptors on the cell surface. To further study the cellular uptake behavior of the nanoparticles, 4T1 cells were treated with FITC loaded nanoparticles for 12 h and then examined by laser scanning confocal microscopy (LSCM). As shown in Fig. 1h and i, Tf-LipoMof@FITC showed the strongest fluorescence intensity when compared with that of the LipoMof@FITC group, suggesting that transferrin did enhance cell uptake process as expected. The targeting ability of transferrin has been proved previously in various applications[22,23] so the increased cellular uptake of

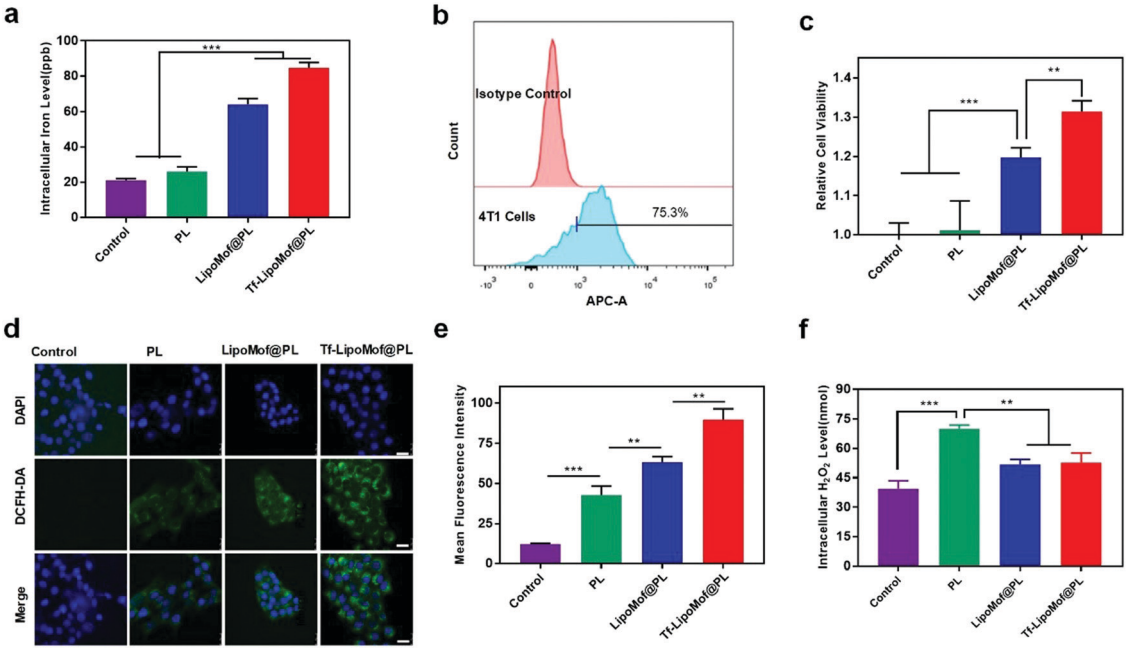

Fig. 2 (a) Detection of the intracellular iron levels of 4T1 cells after incubation with PL, LipoMof@PL and Tf-LipoMof@PL (10 μM calculated by PL) for 6 h (n = 5). (b) Detection of the transferrin receptor (TfR) expression level on 4T1 cells (n = 5). (c) Relative cellular viability of 4T1 cells incubated with PL, LipoMof@PL and Tf-LipoMof@PL (10 μM) in the presence of the TfR antibody (1 μg mL^{-1}) (n = 5). (d) The ROS detected in 4T1 cells after treatment with PL, LipoMof@PL and Tf-LipoMof@PL by using the DCFH-DA assay (scale bar: 50 μm). (e) Semi-quantification of the fluorescence of DCFH-DA (n = 3). (f) Determination of the intracellular H_2O_2 levels in 4T1 cells after incubation with PL, LipoMof@PL and Tf-LipoMof@PL (10 μM) for 6 h (n = 5).

Tf-LipoMof@FITC can be explained by enhanced endocytosis produced by the binding between transferrin and transferrin receptors on the cell surface. Furthermore, the enhanced endocytosis due to transferrin can also lead to higher cytotoxicity which was consistent with previous MTT results.

As the contribution of transferrin to the enhanced cytotoxicity and endocytosis of Tf-LipoMof@PL was confirmed, the transferrin and iron-containing MOF were examined to see if they made Tf-LipoMof@PL a more efficient iron donor. First, as Fig. 2b showed, 75.3% of the population showed positive signal after incubation with the TfR antibody, suggesting the high expression level of TfR on 4T1 cells as previously reported.[18] So, it was concluded that the high level of TfR expression on 4T1 cells provided the prerequisite for transferrin-enhanced iron endocytosis. Next, the facial TfR were blocked by the TfR antibody, and the results showed (Fig. 2c) that cells treated with Tf-LipoMof @PL presented obvious cell viability improvement which can be explained by the fact that after the membrane TfRs were blocked by adding the TfR antibody, the iron intake was greatly compromised which weakened the subsequent cell death caused by iron overloading. To further prove that transferrin played an important role in facilitating the enrichment of the intracellular iron level, ICP-MS was used to determine the intracellular iron level. As Fig. 2a showed, the Tf-LipoMof@PL group also showed the highest intracellular iron level compared with LipoMof@PL. This result reinforced the conclusion drawn from previously mentioned experiments, that transferrin played a pivotal role in enhancing the iron enrichment. As transferrin was proved to be overexpressed in multiple tumor cells, loading transferrin can be an effective targeting method for cancer treatment.[22] Thus, it is believed that transferrin successfully improved the iron endocytosis efficiency and provided crucial conditions for facilitating the iron-induced cell death.

ROS is one of the key factors in promoting lipoperoxidation and play a vital role in various types of cell deaths in which •OH plays a vital role in anticancer therapy.[24] To identify the *in vitro* •OH generation effects of Tf-LipoMof@PL, methylene blue (MB) which can be degraded by •OH was applied to monitor the production of radicals. The H_2O_2 was added as the reactant in the assays because PL cannot generate H_2O_2 *in vitro*. As shown in Fig. S6 (ESI†), the only non-decorated group Mof@PL showed observable MB degradation due to the high levels of •OH generated from Fenton reaction caused by the dissociated Fe ions from uncoated Mof and the added H_2O_2, and the mild degradation effect of the Tf-LipoMof@PL group might be due to the small amount of dissociated Fe iron from the formulation. The results showed that Tf-LipoMof@PL could augment the Fenton reaction to generate •OH with a H_2O_2 donor after dissociation. Piperlongumine was proved to be an efficient H_2O_2 donor *in vivo*.[25] To test if PL-generated H_2O_2 can facilitate the Fenton reaction accompanied by the iron elevation to increase intracellular ROS levels, both H_2O_2 level and the total ROS level after treating cells with different formulations was examined. The titanium sulfate microplate method was used to test intracellular levels of H_2O_2, because titanium sulfate can be specifically oxidized to pertitanic acid by H_2O_2 and then determined by microplate spectrophotometer. The DCFH-DA was used to detect the total intracellular ROS level with CLSM.

In live cells, DCFH-DA would initially be converted to a non-fluorescent intermediate which can be subsequently oxidized by ROS to form fluorescent DCFH to be detected. As Fig. 2f showed, the PL group showed the highest level of H_2O_2. Whereas the total ROS level suggested by DCFH-DA showed different results: the Tf-LipoMof@PL group presented the strongest fluorescence intensity, reflecting the highest amount of ROS generated in Tf-LipoMof@PL (Fig. 2d and e). By comparing the results of the H_2O_2 levels, it was confirmed that PL can produce the highest amount of H_2O_2 when compared with the control, LipoMof@PL and Tf-LipoMof@PL groups with the same PL amount. As the ROS level was highest in Tf-LipoMof@PL, it was presumed that the H_2O_2 generated in Tf-LipoMof@PL was consumed by the Fenton reaction to generate more ROS, resulting in the highest amount of ROS and the lowest H_2O_2 level of the Tf-LipoMof@PL group. Thus, the Tf-LipoMof@PL presented an outstanding ability in synergistic enlargement of ROS generation by combining MOF, transferrin and PL.

Validation of ferroptosis

Because iron-induced ROS elevation can directly induce ferroptosis, Tf-LipoMof@PL was tested to determine if it was an effective ferroptosis inducer. The 4T1 cells were treated with ferrostatin-1 (fer-1, a ferroptosis inhibitor). From the results of the live/dead staining experiment in which dead cells were marked in red and living cells were marked in blue, Tf-LipoMof@PL showed a high degree of cytotoxicity reduction after treating 4T1 cells with fer-1, demonstrating that the cytotoxicity caused by Tf-LipoMof@PL strongly relied on ferroptosis (Fig. 3a). To validate the role of the Fe^{3+} released from the nanoparticles in ferroptosis induction, an iron chelator, DFO was added to the 4T1 cells. Interestingly, the effects of the DFO treatment were different from the effects of fer-1 treatment, and the DFO treated Tf-LipoMof@PL group showed lower cell viability when compared with the LipoMof@PL group. This phenomenon can be explained by that the DFO has a limited iron chelating ability after iron bonding with transferrin compared with that of free iron.[26] Thus, the extra transferrin decorated on the Tf-LipoMof@PL group had prevented a certain amount of Fe^{3+} from being captured by DFO, and this was a strong proof for the contribution of transferrin in the whole ferroptosis-induced nanosystem.

To further validate the pathway of Tf-LipoMof@PL induced ferroptosis, both ferroptosis inhibitors including cysteine (Cys, 2 mM), GSH (2 μM) and α-tocopherol (α-Toc, 25 μM), and ferroptosis inducer glutamic acid (Glu, 2 mM) were used. Fig. 3b shows that all the inhibitors dramatically reduced the cell killing effects of Tf-LipoMof@PL when compared with the free drug. Conversely, Glu as the ferroptosis inducer by inhibiting the intake of Cys achieved the opposite effects. This phenomenon proved that the construction of Tf-LipoMof can effectively facilitate ferroptosis. Western blot analysis was used to test the expression level of intracellular GPX4 which is one of the signs of ferroptosis occurrence. The 4T1 cells were treated with PL, LipoMof@PL and Tf-LipoMof@PL (10 μM, calculated by PL). As Fig. 3d and e showed, Tf-LipoMof@PL had the lowest expression level of GPX4. Correspondingly, the intracellular GSH level of the four groups presented the same pattern (Fig. 3c). Because GSH was the cofactor of GPX4 in lipid peroxidation reduction, the down regulation of GSH caused by PL[25] can contribute to GPX4 down regulation,[27] leading to the deterioration of cellular lipid peroxidation reduction ability and lipid peroxide (LPO) accumulation[28] To further confirm the occurrence of lipid peroxidation in 4T1 cells, intracellular LPO level was determined by using BODIPY-C11, a lipid peroxidation sensor. After treatment with free PL, LipoMof@PL and Tf-LipoMof@PL, the fluorescence intensity in the cells was measured by CLSM. As Fig. 3f and g showed, cells treated with Tf-LipoMof@PL had the highest fluorescence intensity, suggesting the highest level of LPO generation when compared with the LipoMof@PL group, the free drug group and the control. As one of signs of ferroptosis, LPO accumulation was the direct reason for ferroptosis.[7] All the data obtained proved that Tf-LipoMof@PL could induce the ferroptosis pathway by validating the three key factors (GSH decrease, GPX4 down-regulation, LPO accumulation) required for ferroptosis.

Validation of pyroptosis

Previous studies have found that manipulating intracellular iron can also induce pyroptosis. Thus, further studies were made to determine if pyroptosis also contributed to Tf-LipoMof@PL induced cell death. Pyroptosis is a type of cell death mediated by caspase-induced GSDM cleavage with subsequent GSDM pore formation in the cell membrane followed by IL-1β, lactate dehydrogenase (LDH) release and cell bursting.[29] It was reported previously that activating either caspase-1 or caspase-3 pathway can cleave GSDM and induce pyroptosis.[30] To investigate if Tf-LipoMof@PL can induce pyroptosis and which pathway was responsible for Tf-LipoMof@PL induced pyroptosis, 4T1 cells were treated with Ac-DEVD-CHO (DEVD, a caspase-3 inhibitor) and z-YVAD-FMK (YVAD, a caspase-1 inhibitor). As shown in Fig. 3h, cytotoxicity was moderately reduced in the presence of DEVD for cells treated with PL, but not with YVAD treated cells, which suggesting that the free PL induced cell death was more dependent on caspase-3 mediated pathway. As caspase-3 also works in apoptosis, it was presumed that the cell death reduction caused by DEVD was mainly due to the inhibition of PL induced apoptosis.[20] Interestingly, for cells treated with LipoMof@PL and Tf-LipoMof@PL groups, cell cytotoxicity was evidently inhibited by adding YVAD, while no significant difference of cell viability was observed in the presence of DEVD compared with the PL group. This result suggested that the cell death in the LipoMof@PL and Tf-LipoMof@PL group was more influenced by the caspase-1 mediated pathway rather than the caspase-3 mediated one. Because the cleavage of full-long GSDM can be mediated by caspase-1 activation, the reduction of full-long GSDMD can provide further proof for the occurrence of pyroptosis.[29] As shown in Fig. 3k, the western blot analysis suggested that there was a significant reduction in full-long GSDMD expression level in the Tf-LipoMof@PL group when compared with the effects of other formulations. By determining the effects of other pyroptosis markers, such as IL-1β and LDH,

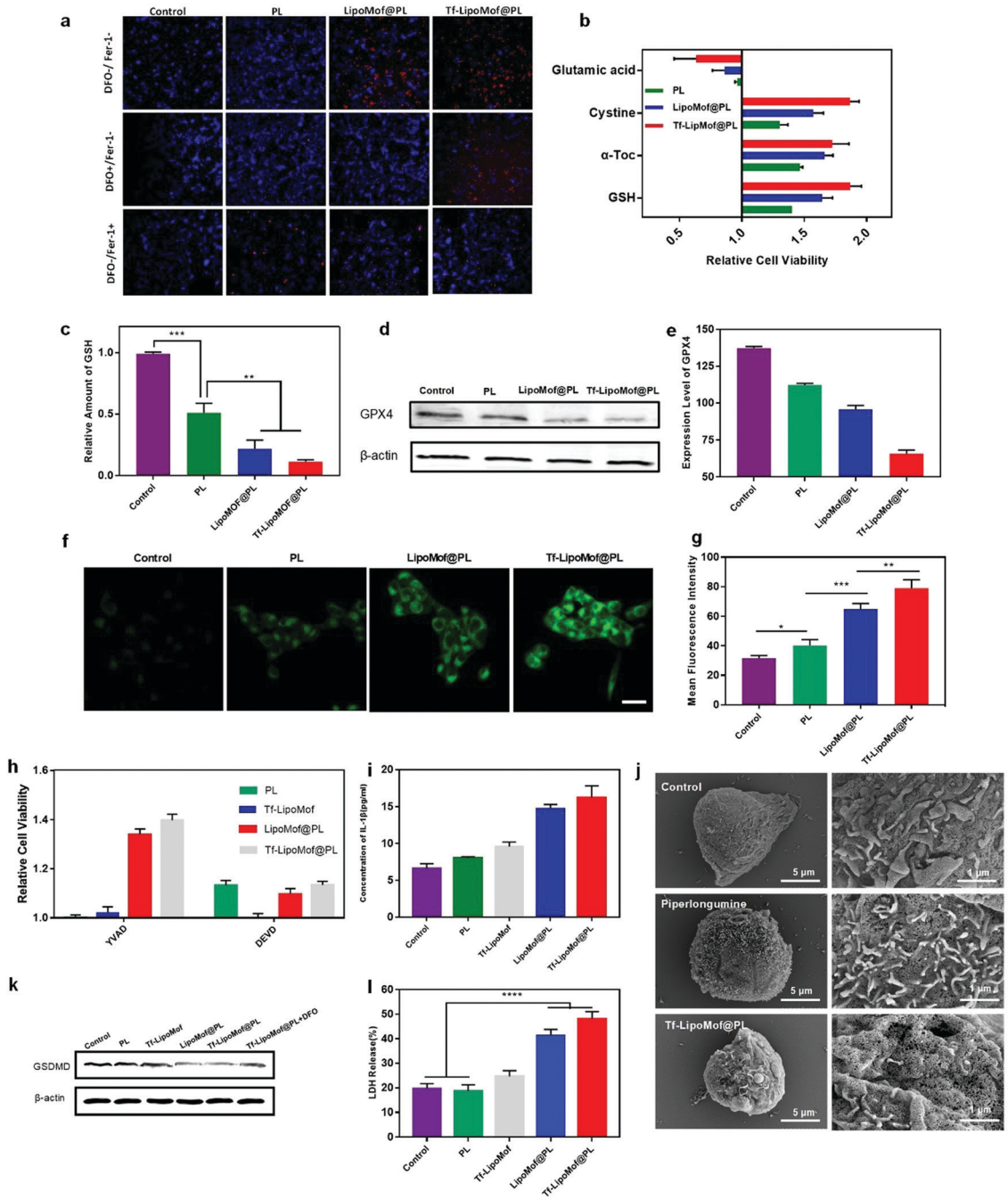

Fig. 3 Validation of the *in vitro* ferroptosis and pyroptosis pathway. (a) Live/dead staining results of 4T1 cells after incubation with different test compounds in the presence of DFO/Fer-1. (b) Relative cell viability (PL, LipoMof@PL and Tf-LipoMof@PL plus various compounds *versus* without compounds) of 4T1 cells after incubation with different groups of preparation (n = 5). (c) Relative intracellular GSH levels of 4T1 cells after treatment with PL, LipoMof@PL and Tf-LipoMof@PL (10 μM) (n = 5). (d and e) Results of western blot analysis and semi-quantification of GPX4 expression in 4T1 cells after the treatment with PL, LipoMof@PL and Tf-LipoMof@PL. (f) LSCM images after BODIY-C11 staining (scale bar: 25 μm), and (g) semi-quantification of 4T1 cells after treatment with PL, LipoMof@PL and Tf-LipoMof@PL (n = 3). (h) Relative cell viability (compared with no inhibitor treatment group) of 4T1 cells treated with of PL, LipoMof@PL and Tf-LipoMof@PL in the presence of either YVAD (caspase-1 inhibitor) or DEVD (caspase-3 inhibitor) (n = 5). (i) Detection of intracellular IL-1β level in 4T1 cells after incubation with PL, LipoMof@PL and Tf-LipoMof@PL (10 μM) for 6 h (n = 5). (j) Morphological changes induced by PL and Tf-LipoMof@PL which were consistent with pyroptosis. (k) Measurement of full-long GSDMD by western blot analysis in 4T1 cells after treatment with PL, LipoMof@PL, Tf-LipoMof@PL (10 μM) and Tf-LipoMof@PL + DFO for 6 h. (l) Detection of LDH level in 4T1 cells after incubation with various preparations (PL = 10 μM) for 6 h (n = 3).

it was shown in Fig. 3i and l that the Tf-LipoMof@PL group presented the highest IL-1β and LDH levels. Meanwhile, the enhanced GSDMD reduction can be reversed by the iron chelator DFO as shown in Fig. 3k, and it was concluded that iron played a part in facilitating the occurrence of pyroptosis. In addition, IL-1β, and LDH levels and GSDMD expression all suggested that

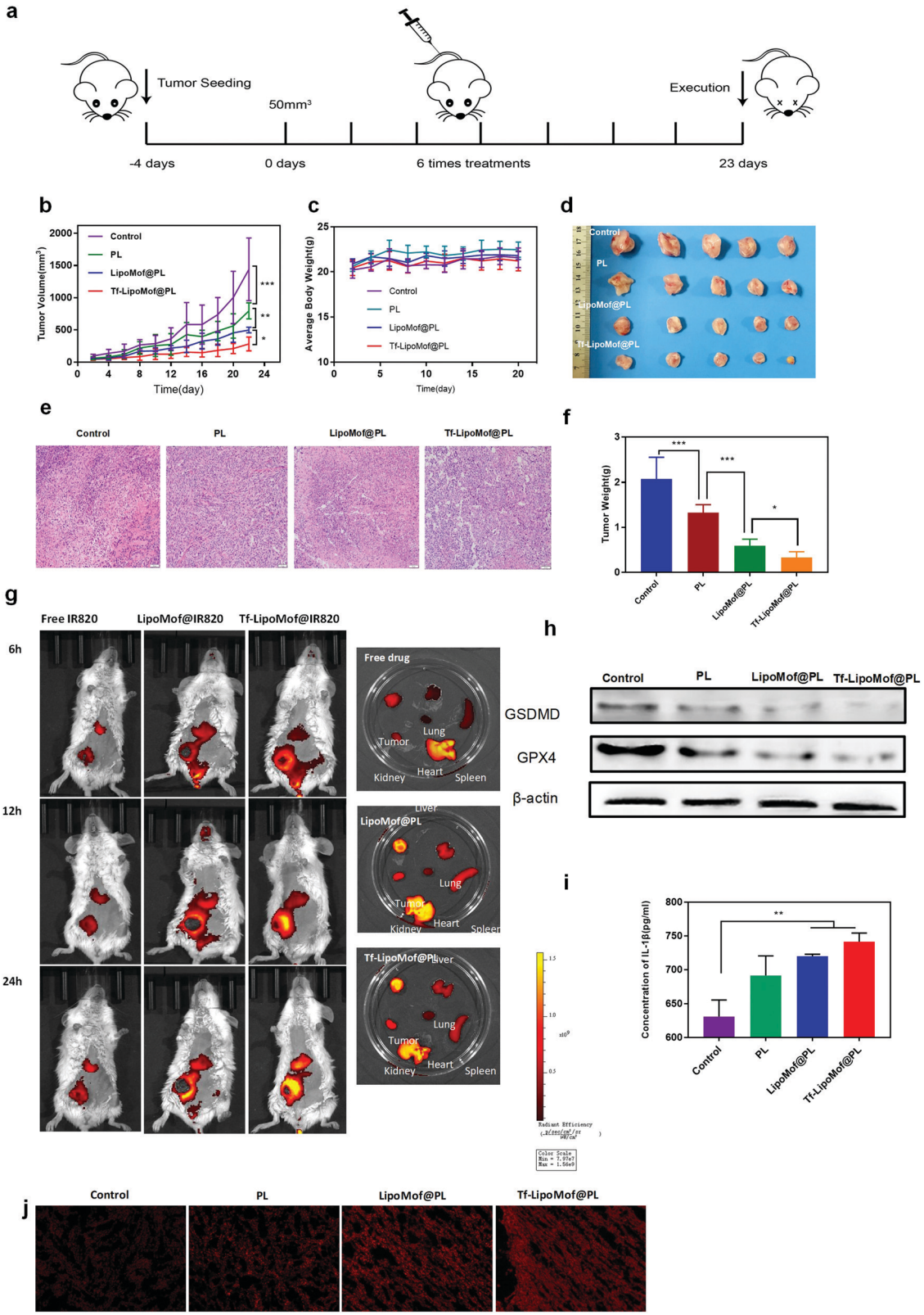

Fig. 4 *In vivo* antitumor efficacy and involvement of ferroptosis/pyroptosis in the therapy. (a) Schematic demonstration of the establishment and treatment of the 4T1-tumor bearing BALB/c mice model. (b) Tumor volume changes (n = 5). (c) Body weight (n = 5). (d) Digital photographs of the dissected tumors (n = 5). (e) The H&E staining of tumor sections in various treatment groups (Scale bars = 100 μm). (f) Tumor weight (n = 5). (g) Bioluminescence images of *in vivo* distribution with different treatments. (h) Measurement of GPX4 and GSDMD expression level by western blot analysis in tumor tissue of different groups. (i) Detection of IL-1β level by ELISA in tumor tissue of different groups (n = 3). (j) Immunofluorescence staining results of ROS levels in the tumors.

Tf-LipoMof without PL also showed pyroptosis inductive effects. This result was in agreement with the results of a previous study, that intracellular iron delivery through an iron containing MOF can induce caspase-1 mediated pyroptosis.[31] Whereas PL as the H_2O_2 donor further facilitated the occurrence of pyroptosis, it was presumed that ROS and iron enrichment triggered by the Tf-LipoMof@PL delivery system played the dominant role which was consistent with a study showing that both ROS and iron enrichment can contribute to the occurrence of pyroptosis.[11] As the GSDMD-mediated membrane pores were one of the signs of pyroptosis,[14] it can also be seen, using scanning electron microscopy, that the Tf-LipoMof@PL treated cells were pock-marked with pores over the entire surface whereas the control group remained intact (Fig. 3j). Thus, it was confirmed that Tf-LipoMof was a good pyroptosis inducer by the results showing that Tf-LipoMof@PL could enhance caspase-1 mediated GSDMD cleavage and increase IL-1β, LDH release.

In vivo anti-tumor effect examination of nanoMofs

As we already proved that Tf-LipoMof@PL can induce both ferroptosis and pyroptosis *in vitro*. It was also speculated that LipoMof@PL could also inhibit tumor growth *in vivo*. For the next part of the study, 4T1 xenograft mice were used to evaluate the anti-tumor efficacy of Tf-LipoMof @PL *in vivo*. Twenty female tumor-bearing mice were randomly separated into four groups and each group was treated with one of the test compounds (saline, PL, LipoMof@PL or Tf-LipoMof@PL) with a fixed dosage (5 mg kg^{-1} calculated by PL) for a 21 days observation (Fig. 4a). First, the tumor growth inhibitory effects were investigated using pharmacodynamics experiments. As shown in Fig. 4b, compared to the saline group, mice treated with free PL, LipoMof@PL or Tf-LipoMof@PL all showed tumor inhibition effect in which Tf-LipoMof@PL treated group suggested the strongest antitumor efficacy. The final tumor volume and the mass of the excised tumors of different groups were consistent with the tumor inhibition behavior (Fig. 4d and f). The biodistribution of different formulations in 4T1-xenografted mouse model were also monitored and PL was replaced with IR820. Then the nanoparticles *in vivo* after intravenous injection were traced (Fig. 4g). The fluorescence signals in nanoparticles decorated with both transferrin and lipid were clearly stronger than those of the lipid-coating group and the free drug group, suggesting that there were tumor-targeting effects of transferrin *in vivo*, which was in agreement with the stronger anti-tumor effects of the Tf-LipoMof@PL group. In addition, no significant systemic toxicity was observed because the body weight of the mice remained steady (Fig. 4c). The histological analysis of the major organs further confirmed that there was no obvious systemic toxicity (Fig. S7, ESI†).

To further investigate if the tumor inhibition effect was attributed to both ferroptosis and pyroptosis, GPX4, GSDMD and IL-1β expression levels in the tumor region were evaluated (Fig. 4h and i). Corresponding to the results of the *in vitro* analysis, GPX4 was obviously downregulated in the tumor site in mice treated with Tf-LipoMof@PL when compared with LipoMof@PL and free PL group, and the immunofluorescence staining results of the tumor slice suggested that the Tf-LipoMof@PL treated group had the highest ROS level (Fig. 4j) which showed that the ferroptosis occurred in Tf-LipoMof@PL group was most observant. The GSDMD level showed the same trend with GPX4 and the Tf-LipoMof@PL group presented the highest IL-1β level. These results all confirmed that pyroptosis also contributed to the anticancer effects.

Conclusion

In summary, dual-inductive Tf-LipoMof@PL nanoparticles were successfully constructed, and achieved promising anti-cancer effects by inducing both ferroptosis and pyroptosis. The iron level was dramatically elevated with the synergizing effects of iron-containing MOF and transferrin-mediated iron endocytosis. Synergizing ROS elevation was also achieved by an enhanced Fenton reaction on the basis of a high amount of H_2O_2 provided by PL piperlongumine (an effective ferroptosis inducer) as well as enriched intracellular iron level. Both *in vitro* and *in vivo* results of Tf-LipoMof@PL demonstrated that ferroptosis and pyroptosis were successfully evoked, and ferroptosis was confirmed by GPX4 depletion and LPO elevation, and pyroptosis was confirmed by enhanced GSDMD cleavage and IL-1β, LDH increase. Moreover, because of the fundamental difference between the ferroptosis/pyroptosis combinational therapy and a traditional anticancer pathway, the novel treatment would provide new choices for anti-cancer therapy. Thus, the ferroptosis/pyroptosis dual-inductive nano delivery system presented is a promising novel anticancer modality with high performance and strong future potential.

Conflicts of interest

There are no conflicts to declare.

Acknowledgements

This work was supported by grants from the National Natural Science Foundation of China (Grant No. 81972812).

References

1 C. Holohan, S. Van Schaeybroeck, D. B. Longley and P. G. Johnston, Cancer drug resistance: an evolving paradigm, *Nat. Rev. Cancer*, 2013, **13**(10), 714–726.
2 G. Housman, S. Byler, S. Heerboth, K. Lapinska, M. Longacre, N. Snyder and S. Sarkar, Drug resistance in cancer: an overview, *Cancers*, 2014, **6**(3), 1769–1792.
3 K. Nurgali, R. T. Jagoe and R. Abalo, Editorial: adverse Effects of Cancer Chemotherapy: anything New to Improve Tolerance and Reduce Sequelae?, *Front. Pharmacol.*, 2018, **9**, 245.
4 R. M. Mohammad, I. Muqbil, L. Lowe, C. Yedjou, H. Y. Hsu, L. T. Lin, M. D. Siegelin, C. Fimognari, N. B. Kumar, Q. P. Dou, H. Yang, A. K. Samadi, G. L. Russo, C. Spagnuolo, S. K. Ray, M. Chakrabarti, J. D. Morre, H. M. Coley, K. Honoki, H. Fujii,

A. G. Georgakilas, A. Amedei, E. Niccolai, A. Amin, S. S. Ashraf, W. G. Helferich, X. Yang, C. S. Boosani, G. Guha, D. Bhakta, M. R. Ciriolo, K. Aquilano, S. Chen, S. I. Mohammed, W. N. Keith, A. Bilsland, D. Halicka, S. Nowsheen and A. S. Azmi, Broad targeting of resistance to apoptosis in cancer, *Semin. Cancer Biol.*, 2015, **35**, S78–S103.

5 M. R. Sepand, S. Ranjbar, I. M. Kempson, M. Akbariani, W. C. A. Muganda, M. Muller, M. H. Ghahremani and M. Raoufi, Targeting non-apoptotic cell death in cancer treatment by nanomaterials: recent advances and future outlook, *Nanomedicine*, 2020, **29**, 102243.

6 G. Yan, M. Elbadawi and T. Efferth, Multiple cell death modalities and their key features (Review), *World Acad. Sci. J.*, 2020, **2**(2), 39–48.

7 S. J. Dixon, K. M. Lemberg, M. R. Lamprecht, R. Skouta, E. M. Zaitsev, C. E. Gleason, D. N. Patel, A. J. Bauer, A. M. Cantley, W. S. Yang, B. Morrison 3rd and B. R. Stockwell, Ferroptosis: an iron-dependent form of nonapoptotic cell death, *Cell*, 2012, **149**(5), 1060–1072.

8 K. Nakamura, T. Kawakami, N. Yamamoto, M. Tomizawa, T. Fujiwara, T. Ishii, H. Harigae and K. Ogasawara, Activation of the NLRP3 inflammasome by cellular labile iron, *Exp. Hematol.*, 2016, **44**(2), 116–124.

9 Z. Zheng and G. Li, Mechanisms and Therapeutic Regulation of Pyroptosis in Inflammatory Diseases and Cancer, *Int. J. Mol. Sci.*, 2020, **21**, 4.

10 S. J. Dixon and B. R. Stockwell, The role of iron and reactive oxygen species in cell death, *Nat. Chem. Biol.*, 2014, **10**(1), 9–17.

11 B. Zhou, J. Y. Zhang, X. S. Liu, H. Z. Chen, Y. L. Ai, K. Cheng, R. Y. Sun, D. Zhou, J. Han and Q. Wu, Tom20 senses iron-activated ROS signaling to promote melanoma cell pyroptosis, *Cell Res.*, 2018, **28**(12), 1171–1185.

12 B. Hassannia, P. Vandenabeele and T., Vanden Berghe, Targeting Ferroptosis to Iron Out Cancer, *Cancer Cell*, 2019, **35**(6), 830–849.

13 Q. Wang, Y. Wang, J. Ding, C. Wang, X. Zhou, W. Gao, H. Huang, F. Shao and Z. Liu, A bioorthogonal system reveals antitumour immune function of pyroptosis, *Nature*, 2020, **579**(7799), 421–426.

14 D. Wu, S. Wang, G. Yu and X. Chen, Cell Death Mediated by the Pyroptosis Pathway with the Aid of Nanotechnology: prospects for Cancer Therapy, *Angew. Chem., Int. Ed.*, 2020, **59**, 2–19.

15 P. Horcajada, R. Gref, T. Baati, P. K. Allan, G. Maurin, P. Couvreur, G. Ferey, R. E. Morris and C. Serre, Metal-organic frameworks in biomedicine, *Chem. Rev.*, 2012, **112**(2), 1232–1268.

16 S. V. Torti and F. M. Torti, Iron and cancer: more ore to be mined, *Nat. Rev. Cancer*, 2013, **13**(5), 342–355.

17 T. R. Daniels, E. Bernabeu, J. A. Rodriguez, S. Patel, M. Kozman, D. A. Chiappetta, E. Holler, J. Y. Ljubimova, G. Helguera and M. L. Penichet, The transferrin receptor and the targeted delivery of therapeutic agents against cancer, *Biochim. Biophys. Acta*, 2012, **1820**(3), 291–317.

18 H. Feng, K. Schorpp, J. Jin, C. E. Yozwiak, B. G. Hoffstrom, A. M. Decker, P. Rajbhandari, M. E. Stokes, H. G. Bender, J. M. Csuka, P. S. Upadhyayula, P. Canoll, K. Uchida, R. K. Soni, K. Hadian and B. R. Stockwell, Transferrin Receptor Is a Specific Ferroptosis Marker, *Cell Rep.*, 2020, **30**(10), 3411.

19 G. Y. Liou and P. Storz, Reactive oxygen species in cancer, *Free Radical Res.*, 2010, **44**(5), 479–496.

20 D. Chen, Y. Ma, P. Li, M. Liu, Y. Fang, J. Zhang, B. Zhang, Y. Hui and Y. Yin, Piperlongumine Induces Apoptosis and Synergizes with Doxorubicin by Inhibiting the JAK2-STAT3 Pathway in Triple-Negative Breast Cancer, *Molecules*, 2019, **24**, 12.

21 X. G. Wang, Q. Cheng, Y. Yu and X. Z. Zhang, Controlled Nucleation and Controlled Growth for Size Predicable Synthesis of Nanoscale Metal-Organic Frameworks (MOFs): a General and Scalable Approach, *Angew. Chem., Int. Ed.*, 2018, **57**(26), 7836–7840.

22 K. B. Johnsen, A. Burkhart, F. Melander, P. J. Kempen, J. B. Vejlebo, P. Siupka, M. S. Nielsen, T. L. Andresen and T. Moos, Targeting transferrin receptors at the blood-brain barrier improves the uptake of immunoliposomes and subsequent cargo transport into the brain parenchyma, *Sci. Rep.*, 2017, **7**(1), 10396.

23 K. B. Johnsen, A. Burkhart, L. B. Thomsen, T. L. Andresen and T. Moos, Targeting the transferrin receptor for brain drug delivery, *Prog. Neurobiol.*, 2019, **181**, 101665.

24 S. J. Kim, H. S. Kim and Y. R. Seo, Understanding of ROS-Inducing Strategy in Anticancer Therapy, *Oxid. Med. Cell. Longevity*, 2019, **2019**, 5381692.

25 E. H. K. Jong-Lyel Roh, J. Jin Young Park, M. Won Kim and B.-H. Kwon, Lee, Piperlongumine selectively kills cancer cells and increases cisplatin antitumor activity in head and neck cancer, *OncoTargets Ther.*, 2014, **5**, 12.

26 P. P. Des Richardson, and Erica Baker, The Effect of the Iron(III) Chelator, Desferrioxamine, on Iron and Transferrin Uptake by the Human Malignant Melanoma Cell, *Cancer Res.*, 1994, 6.

27 W. S. Yang, R. SriRamaratnam, M. E. Welsch, K. Shimada, R. Skouta, V. S. Viswanathan, J. H. Cheah, P. A. Clemons, A. F. Shamji, C. B. Clish, L. M. Brown, A. W. Girotti, V. W. Cornish, S. L. Schreiber and B. R. Stockwell, Regulation of ferroptotic cancer cell death by GPX4, *Cell*, 2014, **156**(1-2), 317–331.

28 F. Ursini and M. Maiorino, Lipid peroxidation and ferroptosis: the role of GSH and GPx4, *Free Radical Biol. Med.*, 2020, **152**, 175–185.

29 J. Shi, W. Gao and F. Shao, Pyroptosis: gasdermin-Mediated Programmed Necrotic Cell Death, *Trends Biochem. Sci.*, 2017, **42**(4), 245–254.

30 T. Bergsbaken, S. L. Fink and B. T. Cookson, Pyroptosis: host cell death and inflammation, *Nat. Rev. Microbiol.*, 2009, **7**(2), 99–109.

31 E. Ploetz, A. Zimpel, V. Cauda, D. Bauer, D. C. Lamb, C. Haisch, S. Zahler, A. M. Vollmar, S. Wuttke and H. Engelke, Metal-Organic Framework Nanoparticles Induce Pyroptosis in Cells Controlled by the Extracellular pH, *Adv. Mater.*, 2020, **32**(19), e1907267.

